Universität Potsdam

Christine Böckmann, Jenny Niebsch

Examination of the nonlinear LIDAR-operator : the influence of inhomogeneous absorbing spheres on the operator

NLD Preprints ; 47

Examination of the nonlinear LIDAR-operator - the influence of inhomogeneous absorbing spheres on the operator [1]

Ch. Böckmann [a,2] J. Niebsch [b]

[a] *Universität Potsdam, Institut für Mathematik, PF 601553, D-14415 Potsdam, Germany*

[b] *Weierstraß Institut für Angewandte Analysis und Stochastik, Mohrenstr. 39, D-10117 Berlin, Germany*

Abstract

The determination of the atmospheric aerosol size distribution is an inverse ill-posed problem. The shape and the material composition of the air-carried particles are two substantial model parameters. Present evaluation algorithms only used an approximation with spherical homogeneous particles. In this paper we propose a new numerically efficient recursive algorithm for inhomogeneous multilayered coated and absorbing particles. Numerical results of real existing particles show that the influence of the two parameters on the model is very important and therefore cannot be ignored.

Key words: Multiwavelength lidar; Aerosol size distribution; Inverse ill-posed problem; Multilayered coated and absorbing aerosol, new recursive algorithm

1 Introduction

Warnings of climate change caused by ozone reduction in the atmosphere have us worried since some years. One reason for ozone destruction is chlorine Cl which comes with CFC in the stratosphere. Moreover, atmospheric aerosol plays an important role for climate and for atmospheric chemistry since chemical reactions take place on the surface of the particles in this part

[1] This work has been partially supported by the Bundesministerium für Bildung, Wissenschaft, Forschung und Technologie (BMBF) under grant 07AF310/2.

[2] Corresponding author. E-mail: bockmann@rz.uni-potsdam.de

of the atmosphere and accelerate the activities of chlorine. Furthermore, the presence of black carbon, the main absorbing component of anthropogenic aerosol, may reduce the cooling effect of aerosol, thus leading to an increase in the greenhouse warming. Such particles come e.g. with volcanic eruptions in the stratosphere or with air pollution of the environment over industrial areas. Hence the knowledge of the aerosol size distribution is necessary to model processes of the ozone chemistry, see e.g. McCormick and Thomason [11].
Since some years multiwavelength lidar measurements can be used to determine the size distributions of tropospheric and stratospheric aerosol. Lidar stands for Light detection and ranging. Multiwavelength lidar sounding can give detailed information about spectra of the optical characteristics of the atmospheric aerosol and its microstructural parameters.
The mathematical model of such a lidar measurement process consists of one nonlinear and two linear integral equations. These are the lidar equation

$$P(\lambda, z) = C(\lambda, z) P_e(\lambda) \beta(\lambda, z) \frac{1}{z^2} exp\{-2 \int_0^z \alpha(\lambda, z') dz'\} \quad , \tag{1}$$

where λ is the wavelenght, z the distance from the lidar, C is the system constant, P_e the intensity of the emitted signal, P the intensity of the detected signal, β is the backscatter coefficient, α the extinction coefficient, and the Fredholm integral equations of first kind for backscatter and extinction coefficient β^{Aer} and α^{Aer}

$$\beta^{Aer}(\lambda, z) = \int_{r_a}^{r_b} r^2 K_\pi(r, \lambda; m) n(r, z)\ dr = \int_{r_a}^{r_b} \pi r^2 Q_\pi(r, \lambda; m) n(r, z)\ dr, \tag{2}$$

$$\alpha^{Aer}(\lambda, z) = \int_{r_a}^{r_b} r^2 K_{ext}(r, \lambda; m) n(r, z)\ dr = \int_{r_a}^{r_b} \pi r^2 Q_{ext}(r, \lambda; m) n(r, z)\ dr, \tag{3}$$

where r is the particle radius, m the particle complex refractive index, n the aerosol size distribution we are looking for, Q_π the backscatter and Q_{ext} the extinction efficiency factors. We have $\beta = \beta^{Aer} + \beta^{Ray}$ and $\alpha = \alpha^{Aer} + \alpha^{Ray}$, where the superscripts Aer and Ray represent the values for aerosol and air molecules, respectively. The values β^{Ray} and α^{Ray} can be evaluated with the air density profile predetermined from either meteorological measurements or other models.
The problem of determining the aerosol size distribution function $n(r, z)$, by multispectral lidar measurements, belongs to the class of inverse ill-posed problems. Given the aerosol backscatter and extinction coefficients at only a few lidar wavelengths it was shown in Müller, Ansmann, Wandinger, Althausen [13] by using an inversion method via regularization with projection and in

Böckmann, Biele, Neuber [2] by using an inversion technique with a mollifier function as regularization parameter, that it is possible, to determine the aerosol size distribution. The last method is able to separate the ill-posedness of the problem from the measurement errors. But all of these inversion algorithms approximate the aerosol consisting of spherical and homogeneous particles, i.e. they used the so called Mie-theorie. In this paper we deal with spherical inhomogeneous multilayered and absorbing particles. Therefore, we have to consider the kernel functions K_π and K_{ext} of the integral equations (2) and (3). The kernel functions reflect shape and material composition of the particles. For absorbing particles the refractive index is complex. The magnitude of the imaginary part of m reflects the degree of absorption. We model the inhomogeneities of a real existing aerosol considering core and cover of a spherical particle and different layers between both. The necessity of an inhomogeneous model was shown in Stämpfli et al [17] since in most cases the aerosol is not a homogeneous one.
The extension of the theory to multilayer sphere is first discussed by Kerker [10] and is straightforward. In the last few years were developed some other possibilities by using different recursive methods for special cases see e.g. Johnson [9] and Wu and Wang [18]. The straightforward method of Kerker [10] rapidly becomes impractical as s, the number of layers, becomes large because of computer memory requirements to store the matrix. Moreover, the time required to solve the $2s$-dimensional linear system with standard procedures is approximately proportional to s^3 and can become excessive. The matrix is a sparse one with a special band structure. Therefore by using standard methods numerical inaccuracies appear because of round-off errors.In this paper we propose an efficient algorithm to determine the backscatter and extinction efficiency factors Q_π and Q_{ext} for spherical inhomogeneous multilayered and absorbing particles. First we will give a short overview of the theoretical background. Second we will develop a new recursion formula for an effective determining of the backscatter and extinction efficiency factors. The implementation with complex refractive indices in the resulting algorithm is new. We will show some numerical results of real existing particles in the atmosphere comparing the non-absorbing and the absorbing model and the homogeneous and inhomogeneous model, respectively.

2 Determination of the efficiency factors

First we want to provide the most important theoretical results of the scattering process of an electromagnetic wave on a sphere. These results are detailed derived in Bohren and Huffman [5] and Kerker [10]. We start with the assumption that the incident wave $(\mathbf{E}_i, \mathbf{H}_i)$ is time harmonic. That means

$$\mathbf{E} = \mathbf{E_0} \exp(i\mathbf{kx} - i\omega t) \quad \text{and} \quad \mathbf{H} = \mathbf{H_0} \exp(i\mathbf{kx} - i\omega t).$$

Each wave, the incident wave, the scattered wave $(\mathbf{E}_s, \mathbf{H}_s)$, and the wave inside the sphere $(\mathbf{E}_1, \mathbf{H}_1)$ (respectively the s waves $(\mathbf{E}_{1j}, \mathbf{H}_{1j}), j = 1, \ldots, s$ if the sphere has s layers) has to satisfy the Maxwell equations. This leads in our case to the conditions

$$\bigtriangledown \mathbf{H} = 0, \quad \bigtriangledown \times \mathbf{E} = i\omega\mu\mathbf{H}, \quad \bigtriangledown \mathbf{E} = 0, \quad \bigtriangledown \times \mathbf{H} = -i\omega\varepsilon\mathbf{E},$$

where μ is the permeability, ε the permittivity, $\omega = (2\pi)/(\lambda)$ and λ the wavelenght. With less effort we obtain the vector wave equations $\triangle\mathbf{E} + k^2\mathbf{E} = \mathbf{0}$ and $\triangle\mathbf{H} + k^2\mathbf{H} = \mathbf{0}$ with $k^2 = \omega^2\varepsilon\mu$. Applying the continuity condition of the tangential electromagnetic field component at the scatterers surface results in the boundary conditions (at the surfaces between neighbouring layers, respectively)

$$\begin{aligned} \Big(\mathbf{E}_i(\mathbf{r}) + \mathbf{E}_s(\mathbf{r}) - \mathbf{E}_1(\mathbf{r})\Big) \times \mathbf{r} &= \mathbf{0} \\ \Big(\mathbf{H}_i(\mathbf{r}) + \mathbf{H}_s(\mathbf{r}) - \mathbf{H}_1(\mathbf{r})\Big) \times \mathbf{r} &= \mathbf{0}, \quad \text{for} \quad \mathbf{r} = \mathbf{R}, \end{aligned}$$

where $\mathbf{R}$ is the sphere radius (the radius of the particular layer, respectively). We make an assumption to the fundamental solutions of the vector wave equation. Let ψ be an arbitrary scalar function and $\mathbf{r}$ the radius vector. We construct two vector functions the so called vector spherical harmonics

$$\mathbf{M} = \bigtriangledown \times (\mathbf{r}\psi) \quad \text{and} \quad \mathbf{N} = \frac{\bigtriangledown \times \mathbf{M}}{k}.$$

Both have the property of beeing divergence-free. The curl of $\mathbf{N}$ is proportional to $\mathbf{M}$ and conversely. If $\mathbf{M}$ satisfies the vector wave equation so does $\mathbf{N}$. Because of

$$\triangle\mathbf{M} + k^2\mathbf{M} = \bigtriangledown \times [\mathbf{r}(\triangle\psi + k^2\psi)] \ ,$$

$\mathbf{M}$ satisfies the vector wave equation if and only if ψ satisfies the scalar wave equation. Therefore we only have to solve the scalar wave equation which we write in spherical coordinates adapted to our problem

$$\frac{1}{r^2}\frac{\partial}{\partial r}(r^2\frac{\partial\psi}{\partial r}) + \frac{1}{r^2\sin\vartheta}\frac{\partial}{\partial\vartheta}(\sin\vartheta\frac{\partial\psi}{\partial\vartheta}) + \frac{1}{r^2\sin^2\vartheta}\frac{\partial^2\psi}{\partial\varphi^2} + k^2\psi = 0.$$

The fundamental solutions of this equation were found with the separation assumption that $\psi(r, \vartheta, \varphi) = R(r)\Theta(\vartheta)\Phi(\varphi)$ and are well known.

$$\psi_{1mn} = \cos(m\varphi)P_n^m(\cos\vartheta)Z_n(kr), \quad \psi_{2mn} = \sin(m\varphi)P_n^m(\cos\vartheta)Z_n(kr),$$

where m is a positive integer, P_n^m is the Legendre function of degree m and order n and Z_n is one of the Ricatti-Bessel functions

$$\psi_n(z) = zj_n(z), \quad \chi_n(z) = zy_n(z), \quad \zeta_n(z) = \psi(z) + \chi(z)i, \tag{4}$$

with the spherical Bessel functions j_n and y_n. Now we can determine $\mathbf{M}_{1mn}, \mathbf{M}_{2mn}, \mathbf{N}_{1mn}$ and $\mathbf{N}_{2mn}$. Writing the electromagnetic wave as series in $\mathbf{M}$ and $\mathbf{N}$ we get for the known incident wave

$$\begin{aligned}
\mathbf{E}_i &= E_0 \sum_{n=1}^{\infty} i^n \frac{2n+1}{n(n+1)} (\mathbf{M}_{21n} - i\mathbf{N}_{11n}), \\
\mathbf{H}_i &= -\frac{k}{\omega\mu} E_0 \sum_{n=1}^{\infty} i^n \frac{2n+1}{n(n+1)} (\mathbf{M}_{11n} + i\mathbf{N}_{21n}).
\end{aligned}$$

The inside wave and the scattering wave we are looking for can be written as

$$\begin{aligned}
\mathbf{E}_1 &= E_0 \sum_{n=1}^{\infty} i^n \frac{2n+1}{n(n+1)} (c_n\mathbf{M}_{21n} - id_n\mathbf{N}_{11n}), \\
\mathbf{H}_1 &= -\frac{k}{\omega\mu} E_0 \sum_{n=1}^{\infty} i^n \frac{2n+1}{n(n+1)} (d_n\mathbf{M}_{11n} + ic_n\mathbf{N}_{21n}),
\end{aligned}$$

and

$$\begin{aligned}
\mathbf{E}_s &= E_0 \sum_{n=1}^{\infty} i^n \frac{2n+1}{n(n+1)} (-b_n\mathbf{M}_{21n} + ia_n\mathbf{N}_{11n}), \\
\mathbf{H}_s &= \frac{k}{\omega\mu} E_0 \sum_{n=1}^{\infty} i^n \frac{2n+1}{n(n+1)} (a_n\mathbf{M}_{11n} + ib_n\mathbf{N}_{21n}).
\end{aligned}$$

Following formulas hold for extinction, scatter and backscatter efficiency factors, see Bohren and Huffman [5],

$$\begin{aligned}
Q_{ext} &= \frac{2}{k^2r^2} \sum_{n=1}^{\infty} (2n+1) Re(a_n + b_n), \\
Q_{sca} &= \frac{2}{k^2r^2} \sum_{n=1}^{\infty} (2n+1)(|a_n|^2 + |b_n|^2), \\
Q_{\pi} &= \frac{1}{k^2r^2} |\sum_{n=1}^{\infty} (2n+1)(-1)^n (a_n - b_n)|^2
\end{aligned}$$

with $k = 2\pi/\lambda$. Hence we are interested in the scattering coefficients a_n and b_n. Substituting the founded waves in the boundary conditions we obtain in general a linear equation system in a_n and c_n and another one in d_n and b_n and

we solve both, first one for a_n, second one for b_n.Firstly, for a homogeneous sphere holds

$$a_n = \frac{m_1\psi_n(m_1\alpha_1)\psi_n'(\alpha_1) - \psi_n(\alpha_1)\psi_n'(m_1\alpha_1)}{m_1\psi_n(m_1\alpha_1)\zeta_n'(\alpha_1) - \zeta_n(\alpha_1)\psi_n'(m_1\alpha_1)}$$
$$b_n = \frac{\psi_n(m_1\alpha_1)\psi_n'(\alpha_1) - m_1\psi_n(\alpha_1)\psi_n'(m_1\alpha_1)}{\psi_n(m_1\alpha_1)\zeta_n'(\alpha_1) - m_1\zeta_n(\alpha_1)\psi_n'(m_1\alpha_1)}.$$

Secondly, for a multilayered sphere the number of boundary conditions and hence the number of equations raises in accordance. For a s-layered sphere we get two systems of dimension $2s$, one for a_n and one for b_n, of the following structure

$$\mathbf{A}\ (x_1, x_2, ..., x_{2s-1}, a_n)^T \quad = \quad (0, ..., 0, \psi_n'(\alpha_l), \psi_n(\alpha_l))^T$$

where $\mathbf{A}$ has the structure

$$\begin{pmatrix}
\psi_n'(m_1\alpha_1) & \psi_n'(m_2\alpha_1) & \chi_n'(m_2\alpha_1) & 0 & 0 & \ldots & 0 \\
m_1\psi_n(m_1\alpha_1) & m_2\psi_n(m_2\alpha_1) & m_2\chi_n(m_2\alpha_1) & 0 & 0 & \ldots & 0 \\
0 & \psi_n'(m_2\alpha_2) & \chi_n'(m_2\alpha_2) & \psi_n'(m_3\alpha_2) & \chi_n'(m_3\alpha_2) & \ldots & 0 \\
0 & m_2\psi_n(m_2\alpha_2) & m_2\chi_n(m_2\alpha_2) & m_3\psi_n(m_3\alpha_2) & m_3\chi_n(m_3\alpha_2) & \ldots & 0 \\
0 & 0 & 0 & \psi_n'(m_3\alpha_3) & \chi_n'(m_3\alpha_3) & \ldots & 0 \\
\ldots & & & & & & \\
\ldots & & & 0 & 0 \ \psi_n'(m_l\alpha_l) & \chi_n'(m_l\alpha_l) & \zeta_n'(\alpha_l) \\
\ldots & & & 0 & 0 \ m_l\psi_n(m_l\alpha_l) & m_l\chi_n(m_l\alpha_l) & \zeta_n(\alpha_l)
\end{pmatrix}$$

or shorter, respectively

$$\begin{pmatrix}
a_{11} & a_{12} & a_{13} & 0 & 0 & \ldots & 0 \\
a_{21} & a_{22} & a_{23} & 0 & 0 & \ldots & 0 \\
0 & a_{32} & a_{33} & a_{34} & a_{35} & \ldots & 0 \\
0 & a_{42} & a_{43} & a_{44} & a_{45} & \ldots & 0 \\
0 & 0 & 0 & a_{54} & a_{55} & \ldots & 0 \\
\ldots & & & & & & \\
\ldots & a_{2s-5\ 2s-5} & a_{2s-5\ 2s-4} & a_{2s-5\ 2s-3} & 0 & 0 & 0 \\
\ldots & a_{2s-4\ 2s-5} & a_{2s-4\ 2s-4} & a_{2s-4\ 2s-3} & 0 & 0 & 0 \\
\ldots & 0 & a_{2s-3\ 2s-4} & a_{2s-3\ 2s-3} & a_{2s-3\ 2s-2} & a_{2s-3\ 2s-1} & 0 \\
\ldots & 0 & a_{2s-2\ 2s-4} & a_{2s-2\ 2s-3} & a_{2s-2\ 2s-2} & a_{2s-2\ 2s-1} & 0 \\
\ldots & 0 & 0 & 0 & a_{2s-1\ 2s-2} & a_{2s-1\ 2s-1} & a_{2s-1\ 2s} \\
\ldots & 0 & 0 & 0 & a_{2s\ 2s-2} & a_{2s\ 2s-1} & a_{2s\ 2s}
\end{pmatrix} \tag{5}$$

The coefficients of the matrix are Bessel functions, see (4), with the refractive indices m_i, the radii r_i and the size parameters $\alpha_i = kr_i (i = 1, ..., s)$. For more details see Kerker [10]. Solving such a system for a_n or b_n, respectively, we can

adapt well-known numerical procedures to the special matrix form. In this way we can reduce the requirement of time e.g. by using special implizit Givens rotations proportional to $38s$ multiplications and 6 square root operations and by using a special Gauss algorithm proportional to $8s$ multiplications.

3 Development of an efficient recursive algorithm

The band structure of the matrix **A** also suggests to try an expansion of the determinant to solve the problem. We will show that in this way by finding a recursion formula the time requirement can be reduced proportional to $4s$ multiplications.

Proposition 1 *Let A_s be a matrix of dimension $2s$ of the structure (5). The determinant $|A_s|$ of A_s can be determine by*

$$|A_s| = x_{2s-2} \begin{vmatrix} a_{2s-1\ 2s-1} & a_{2s-1\ 2s} \\ a_{2s\ 2s-1} & a_{2s\ 2s} \end{vmatrix} + y_{2s-2} \begin{vmatrix} a_{2s-1\ 2s-2} & a_{2s-1\ 2s} \\ a_{2s\ 2s-2} & a_{2s\ 2s} \end{vmatrix},$$

where $x_1 = a_{11}, y_1 = -a_{21}$,

$$\left.\begin{aligned} x_i &= x_{i-1}a_{ii} + y_{i-1}a_{i\ i-1} \\ y_i &= x_{i-1}(-a_{i+1\ i}) + y_{i-1}(-a_{i+1\ i-1}) \end{aligned}\right\} \quad \textit{for } i \textit{ odd}, \tag{6}$$

and

$$\left.\begin{aligned} x_i &= x_{i-1}a_{ii} + y_{i-1}a_{i-1\ i} \\ y_i &= x_{i-1}(-a_{i\ i+1}) + y_{i-1}(-a_{i-1\ i+1}) \end{aligned}\right\} \quad \textit{for } i \textit{ even}, \tag{7}$$

$$i = 2, \ldots, 2s-2. \tag{8}$$

Proof: We proof the proposition by induction and start with $s = 3$. First we expand $|A_3|$ with respect to the first column

$$|A_3| = a_{11} \begin{vmatrix} a_{22} & a_{23} & 0 & 0 & 0 \\ a_{32} & a_{33} & a_{34} & a_{35} & 0 \\ a_{42} & a_{43} & a_{44} & a_{45} & 0 \\ 0 & 0 & a_{54} & a_{55} & a_{56} \\ 0 & 0 & a_{64} & a_{65} & a_{66} \end{vmatrix} - a_{21} \begin{vmatrix} a_{12} & a_{13} & 0 & 0 & 0 \\ a_{32} & a_{33} & a_{34} & a_{35} & 0 \\ a_{42} & a_{43} & a_{44} & a_{45} & 0 \\ 0 & 0 & a_{54} & a_{55} & a_{56} \\ 0 & 0 & a_{64} & a_{65} & a_{66} \end{vmatrix}.$$

We now expand both determinants with respect to the first row. We get four new determinants where particular two are identical. Summarizing the coefficients we get

$$|A_3| = (a_{11}a_{22} - a_{21}a_{12}) \begin{vmatrix} a_{33} & a_{34} & a_{35} & 0 \\ a_{43} & a_{44} & a_{45} & 0 \\ 0 & a_{54} & a_{55} & a_{56} \\ 0 & a_{64} & a_{65} & a_{66} \end{vmatrix} + (a_{11}(-a_{23}) + a_{21}a_{13}) \begin{vmatrix} a_{32} & a_{34} & a_{35} & 0 \\ a_{42} & a_{44} & a_{45} & 0 \\ 0 & a_{54} & a_{55} & a_{56} \\ 0 & a_{64} & a_{65} & a_{66} \end{vmatrix}.$$

We repeat these two steps summerizing in each step the corresponding coefficients and obtain $|A_3| = u_1 \begin{vmatrix} a_{55} & a_{56} \\ a_{65} & a_{66} \end{vmatrix} + u_2 \begin{vmatrix} a_{54} & a_{56} \\ a_{64} & a_{66} \end{vmatrix}$, with

$$\begin{aligned} u_1 = & a_{11}a_{22}a_{33}a_{44} - a_{21}a_{12}a_{33}a_{44} - a_{11}a_{23}a_{32}a_{44} + a_{21}a_{13}a_{32}a_{44} \\ & -a_{11}a_{22}a_{43}a_{34} + a_{21}a_{12}a_{43}a_{34} + a_{11}a_{23}a_{42}a_{34} - a_{21}a_{13}a_{42}a_{34}, \\ u_2 = & -a_{11}a_{22}a_{33}a_{45} + a_{21}a_{12}a_{33}a_{45} + a_{11}a_{23}a_{32}a_{45} - a_{21}a_{13}a_{32}a_{45} \\ & +a_{11}a_{22}a_{43}a_{35} - a_{21}a_{12}a_{43}a_{35} - a_{11}a_{23}a_{42}a_{35} + a_{21}a_{13}a_{42}a_{35}. \end{aligned}$$

It is easy to verify that using the recursion formula for $s = 3$ we have $x_4 = u_1$ and $y_4 = u_2$. Now we assume the formula holds for s. We will show the correctness for $s+1$ where we have to consider the matrix

$$|A_{s+1}| = \begin{vmatrix} & & | & \vdots & \vdots & \vdots & \vdots \\ & A_{s-1} & | & 0 & 0 & 0 & 0 \\ & & | & a_{2s-3\ 2s-1} & 0 & 0 & 0 \\ & - - - - - & & a_{2s-2\ 2s-1} & 0 & 0 & 0 \\ \cdots & 0 & a_{2s-1\ 2s-2} & a_{2s-1\ 2s-1} & a_{2s-1\ 2s} & a_{2s-1\ 2s+1} & 0 \\ \cdots & 0 & a_{2s\ 2s-2} & a_{2s\ 2s-1} & a_{2s\ 2s} & a_{2s\ 2s+1} & 0 \\ \cdots & 0 & 0 & 0 & a_{2s+1\ 2s} & a_{2s+1\ 2s+1} & a_{2s+1\ 2s+2} \\ \cdots & 0 & 0 & 0 & a_{2s+2\ 2s} & a_{2s+2\ 2s+1} & a_{2s+2\ 2s+2} \end{vmatrix}.$$

We expand $|A_{s+1}|$ with respect to the last column

$$|A_{s+1}| = a_{2s+2\ 2s+2} \begin{vmatrix} & & | & \vdots & \vdots & \vdots \\ & A_{s-1} & | & 0 & 0 & 0 \\ & & | & a_{2s-3\ 2s-1} & 0 & 0 \\ & - - - - - & & a_{2s-2\ 2s-1} & 0 & 0 \\ \cdots & 0 & a_{2s-1\ 2s-2} & a_{2s-1\ 2s-1} & a_{2s-1\ 2s} & a_{2s-1\ 2s+1} \\ \cdots & 0 & a_{2s\ 2s-2} & a_{2s\ 2s-1} & a_{2s\ 2s} & a_{2s\ 2s+1} \\ \cdots & 0 & 0 & 0 & a_{2s+1\ 2s} & a_{2s+1\ 2s+1} \end{vmatrix} \cdots$$

$$-a_{2s+1\ 2s+2}\begin{vmatrix} & & | & \vdots & \vdots & \vdots \\ & A_{s-1} & | & 0 & 0 & 0 \\ & & | & a_{2s-3\ 2s-1} & 0 & 0 \\ & - - - - - & & a_{2s-2\ 2s-1} & 0 & 0 \\ \cdots & 0 & a_{2s-1\ 2s-2} & a_{2s-1\ 2s-1} & a_{2s-1\ 2s} & a_{2s-1\ 2s+1} \\ \cdots & 0 & a_{2s\ 2s-2} & a_{2s\ 2s-1} & a_{2s\ 2s} & a_{2s\ 2s+1} \\ \cdots & 0 & 0 & 0 & a_{2s+2\ 2s} & a_{2s+2\ 2s+1} \end{vmatrix}.$$

Now we expand both new determinants with respect to the last row. We get

$$|A_{s+1}| = c_1\begin{vmatrix} & & | & \vdots & \vdots \\ & A_{s-1} & | & 0 & 0 \\ & & | & a_{2s-3\ 2s-1} & 0 \\ & - - - - - & & a_{2s-2\ 2s-1} & 0 \\ \cdots & 0 & a_{2s-1\ 2s-2} & a_{2s-1\ 2s-1} & a_{2s-1\ 2s+1} \\ \cdots & 0 & a_{2s\ 2s-2} & a_{2s\ 2s-1} & a_{2s\ 2s+1} \end{vmatrix} + c_2\begin{vmatrix} & & | & \vdots & \vdots \\ & A_{s-1} & | & 0 & 0 \\ & & | & a_{2s-3\ 2s-1} & 0 \\ & - - - - - & & a_{2s-2\ 2s-1} & 0 \\ \cdots & 0 & a_{2s-1\ 2s-2} & a_{2s-1\ 2s-1} & a_{2s-1\ 2s} \\ \cdots & 0 & a_{2s\ 2s-2} & a_{2s\ 2s-1} & a_{2s\ 2s} \end{vmatrix},$$

where $c_1 = a_{2s+2\ 2s+2}(-a_{2s+1\ 2s}) + a_{2s+1\ 2s+2}\, a_{2s+2\ 2s}$ and $c_2 = a_{2s+2\ 2s+2}\, a_{2s+1\ 2s+1} - a_{2s+1\ 2s+2}\, a_{2s+2\ 2s+1}$. We write for the first determinant $|A_s^1|$, for the second $|A_s^2|$. It is easy to see that we can write c_1 and c_2 as determinants, too.

$$|A_{s+1}| = -\begin{vmatrix} a_{2s+1\ 2s} & a_{2s+1\ 2s+2} \\ a_{2s+2\ 2s} & a_{2s+2\ 2s+2} \end{vmatrix}|A_s^1| + \begin{vmatrix} a_{2s+1\ 2s+1} & a_{2s+1\ 2s+2} \\ a_{2s+2\ 2s+1} & a_{2s+2\ 2s+2} \end{vmatrix}|A_s^2|.$$

A_s^1 and A_s^2 are matrices of dimension $2s$. Thus we can use the induction assumption and get

$$|A_s^1| = x_{2s-2}\begin{vmatrix} a_{2s-1\ 2s-1} & a_{2s-1\ 2s+1} \\ a_{2s\ 2s-1} & a_{2s\ 2s+1} \end{vmatrix} + y_{2s-2}\begin{vmatrix} a_{2s-1\ 2s-2} & a_{2s-1\ 2s+1} \\ a_{2s\ 2s-2} & a_{2s\ 2s+1} \end{vmatrix}$$

and

$$|A_s^2| = x_{2s-2}\begin{vmatrix} a_{2s-1\ 2s-1} & a_{2s-1\ 2s} \\ a_{2s\ 2s-1} & a_{2s\ 2s} \end{vmatrix} + y_{2s-2}\begin{vmatrix} a_{2s-1\ 2s-2} & a_{2s-1\ 2s} \\ a_{2s\ 2s-2} & a_{2s\ 2s} \end{vmatrix}.$$

We determine the determinants for A_s^1 and get $|A_s^1| = x_{2s-2}\, a_{2s-1\ 2s-1}\, a_{2s\ 2s+1} - x_{2s-2}\, a_{2s-1\ 2s+1}\, a_{2s\ 2s-1} + y_{2s-2}\, a_{2s-1\ 2s-2}\, a_{2s\ 2s+1} - y_{2s-2}\, a_{2s-1\ 2s+1} - a_{2s\ 2s-2}$. Let $i = 2s-1$ this fits the recursion formula for odd numbers and we have

$$|A_s^1| = (x_{2s-2}\ a_{2s-1\ 2s-1} + y_{2s-2}\ a_{2s-1\ 2s-2})\ a_{2s\ 2s+1}$$

$$
\begin{aligned}
&-(x_{2s-2}\ a_{2s\ 2s-1} + y_{2s-2}\ a_{2s\ 2s-2})\ a_{2s-1\ 2s+1} \\
&= x_{2s-1}\ a_{2s\ 2s+1} + y_{2s-1}\ a_{2s-1\ 2s+1} \\
&= -y_{2s}.
\end{aligned}
$$

In the same way we get $|A_s^2| = x_{2s}$. Hence we get

$$
|A_{s+1}| = x_{2s} \begin{vmatrix} a_{2s+1\ 2s+1} & a_{2s+1\ 2s+2} \\ a_{2s+2\ 2s+1} & a_{2s+2\ 2s+2} \end{vmatrix} + y_{2s} \begin{vmatrix} a_{2s+1\ 2s} & a_{2s+1\ 2s+2} \\ a_{2s+2\ 2s} & a_{2s+2\ 2s+2} \end{vmatrix}.
$$

This is the proposition for A_{s+1}.

4 Numerical results

4.1 Comparison between homogeneous and inhomogeneous model

Unlike tropospheric aerosols one can divide stratospheric aerosols in three main classes. Firstly, backgroundaerosols are aerosols in the tropopause up to ten kilometers height which even exist a long time after volcanic eruptions. They consist of diluted sulfuric acid and probably arise by oxidation of sulphurous gases. Secondly, volcanic aerosols are distributed over the global stratosphere after strong, intensive volcanic eruptions. They consist of sulfuric acid droplets. The presence of such aerosols in the stratosphere exponential decreases with time constants of one year. Thirdly, Polar Stratospheric Clouds (PSC) are a pol region phenomenon. They originate by freezing of water and a mixture of water and nitrid acid. PSC are important for the heterogenic reactions mentioned in the introduction. Besides this rough classification especially PSC have to devide into subclasses. Waterice always appears with strong depolarisation and is described by PSC type II. The arctic is dominated by PSC type I, a mixture of nitrid acid and other trace gases, because the stratospheric freezing temperature is seldom reached. Here we have both, depolarised (type Ia) and non-depolarised PSC (type Ib). Their origin and composition are in discussion and should be derived from existing lidar datas. The homogeneous model consist of a homogeneous mixture of the two different components. An average index of refraction for the mixed components is then obtained from the well-known Lorentz-Lorenz formula
$m_{mix} = (\sqrt{m_1^2\ V_1\ +\ m_2^2\ V_2})/(V_1 + V_2)$ where V_1 and V_2 are the volumes of the two shells. On the other side the inhomogeneous model consists of a core and a cover of different refractive indices m_1 and m_2. Now we follow the suggestion of [17] to model PSC II and assume a nitrit acid trihydrate (NAT) core with a refractive index of 1.5 and a radius of $1\mu m$ and a core of waterice with refractive index 1.31 and variable radius from $1\mu m$ to $6\mu m$, which corresponds

to the growth of these particles. The wavelength is $0.9\mu m$. Comparing the homogeneous and the inhomogeneous model we get the same results as [17]. For PSC II the behavior of the kernel functions for the inhomogeneous model is different from this for the homogeneous model, see figure 1 and 2. More precisely, for the extinction kernel, see figure 1 (left) and 2 (left), a shift and a frequency sweep between both curves lead to a nearly opposite behavior of the two models. Maxima are reached for the first model where minima occur for the second model. The amplitudes differ sometimes by a factor of 2 and more. Differences between both models become drastic in the backscatter kernel, see figure 1 (right) and 2 (right) and reach sometimes a factor of 30. The rather unstructured behavior of the backscatter kernel with radius between $1\mu m$ to $2.5\mu m$ is quite unusual compared to typical sharp Mie-backscatter resonances. It is caused by interference.

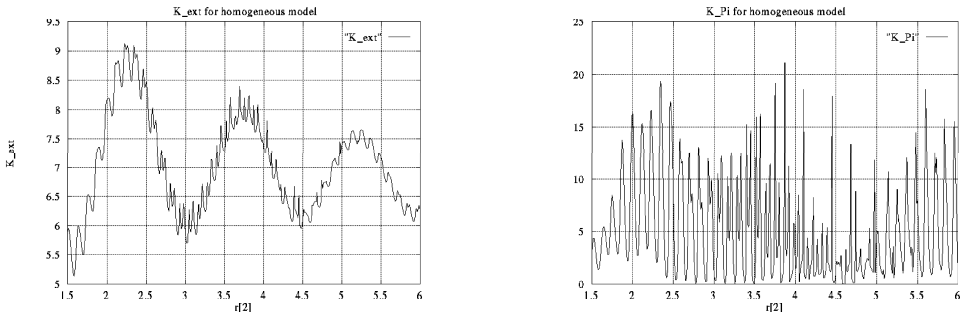

Fig. 1. Homogeneous non-absorbing model.

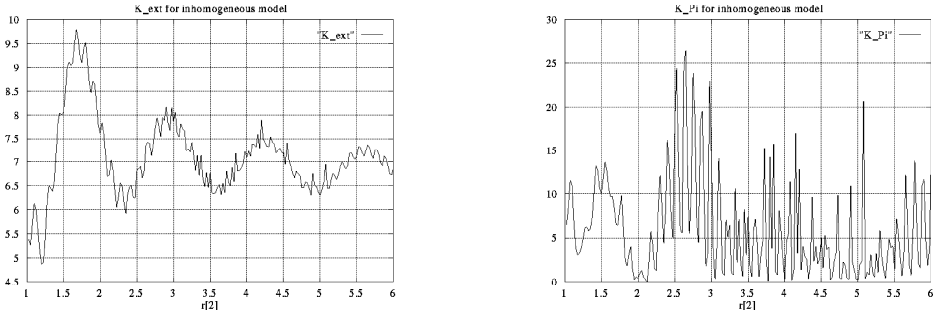

Fig. 2. Inhomogeneous non-absorbing model.

4.2 Examination of absorbing shell particles

Baumgardner et al [1] developed an instrument for airborne in situ measurements of aerosol size and refractive index m. This measure of m can used to

deduce the composition of the particles with some a priori knowledge, e.g. in the stratosphere where the sulfuric acid is thought to be the primary aerosol part. They also have shown the presence of non-spherical or absorbing particles. Moreover, the refractive index depends on the wavelength λ and on the relative humidity. The lower m values represent lower H_2SO_4 mixing ratios associated with larger water vapor. Average stratospheric refractive indices are between 1.34 to 1.46 and the imaginary part is $0.05i$, whereas Rosen et al [14] measured an average between 1.33 to 1.59 but for the imaginary part only $0.006i$. However, particles with even small soot inclusions can be highly absorbing, see Chylek et al [6], such that an assumed imaginary part of $0.05i$ is not necessarily extreme. Because anthropogenic sulfate and black carbon emissions have common sources, anthropogenic aerosol contains a mixture of both, see Schult et al [16]. They measured an average for sulfate between 1.30 to 1.46 and for the imaginary part between $10^{-1}i$ to $10^{-9}i$. Moreover, for black carbon they observed between 1.75 to 2.21 and between $0.43i$ to $0.72i$. Finally, we found by Yoon and Won [19] a real part about 1.5 and an imaginary part between $0.0169i$ to $0.11i$.

Firstly, if we assume weak pollutions of the core ($m_1 = 1.5 + 0.01i$) we hardly have differences for both extinction and backscatter kernel. If we add weak pollutions in the cover ($m_2 = 1.31 + 0.01i$) the backscatter kernel visible decreases, see figure 2 (right) and 3 (right). More precisely, the amplitudes of the backscatter kernels with radius between $1\mu m$ to $2\mu m$ differ by a factor of 2 and between $2\mu m$ to $3\mu m$ by about a factor of 3. Furthermore, between $3\mu m$ to $6\mu m$ the behavior of the backscatter kernels is extremely different.

Small soot inclusions in the core can be highly absorbing. We take $m_1 =$

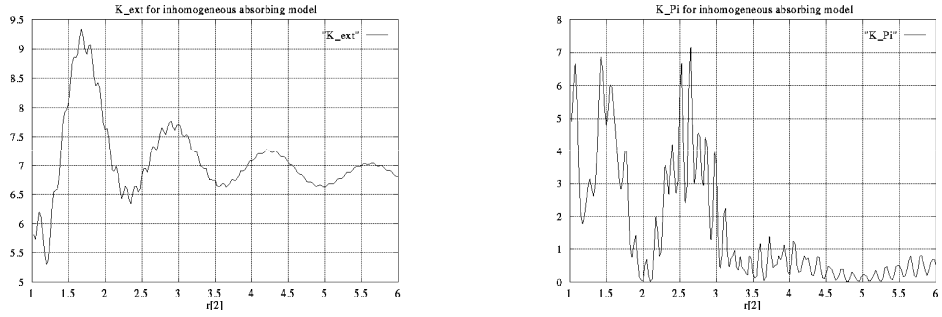

Fig. 3. Weak absorbing core and cover.

$1.5 + 0.05i$, see figure 2, 3 and 4. Whereas in all 3 above mentioned cases the sensitiveness of the extinction kernel is very small, the sensitiveness of the backscatter kernel is important. It seems that an absorbing cover has a larger influence on the backscatter kernel.

Secondly, we can assume particles in the troposphere over industrial areas as highly absorbing. Therefore we suggest a strong absorbing core and weak absorbing cover. For a wavelenght of $\lambda = 0.532\mu m$ we choose $m_1 = 1.7 + 0.1i$

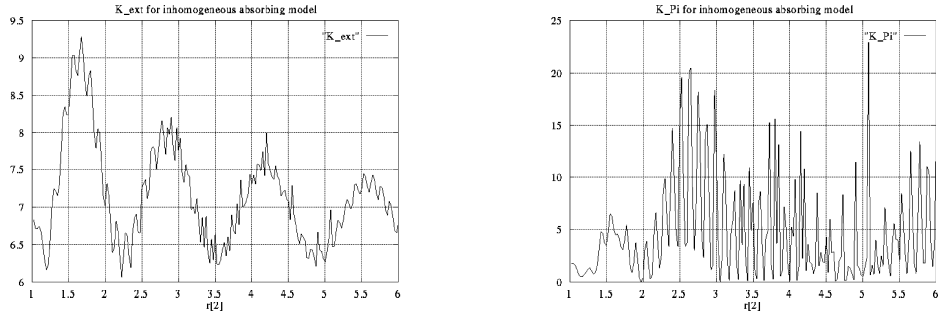

Fig. 4. Strong absorbing core, non-absorbing cover.

and $m_2 = 1.4+0.5*10^{-2}i$. The core radius is $0.5\mu m$ and the cover radius varies between $1\mu m$ to $10\mu m$, see figure 5 (left). If the cover has nearly no absorption (water cover with $m_2 = 1.33+0.5*10^{-8}i$) we get the figure 5 (right). Whereas the extinction kernel is only weak shifted the backscatter kernel behavior is extremely different i.e. incomparable since the particles have different absorbing covers.

There is the suggestion to reverse the ratio, too, and assume weak absorbing

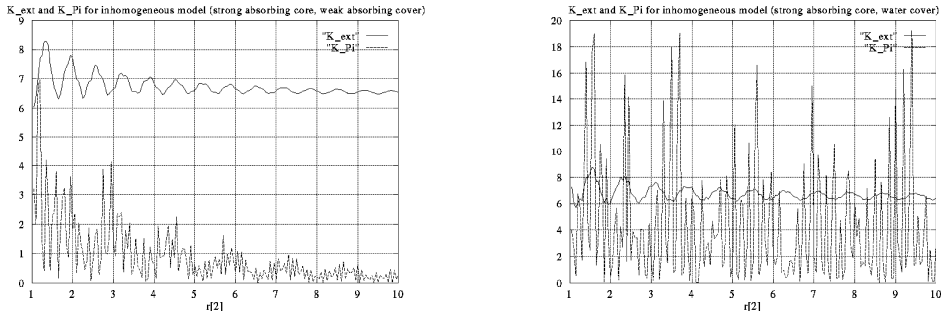

Fig. 5. Strong absorbing core and weak absorbing cover.

core and strong absorbing cover. The numerical results of this case are shown in figure 6. Here we take $m_1 = 1.7+1*10^{-2}i$ and $m_2 = 1.4+0.1i$. However, if we have a strong absorbing cover then both kernels have extremely different properties.

4.3 A model for inhomogeneous aerosol

In the last section we model the inhomogeneity considering core and cover of a spherical particle. Without an interface between them the refractive index inside the particle drops abruptly. Such a step in the refractive index, however, cannot reproduce an actual particle satisfactorily. In order to estimate the effect of a continuous gradient in the refractive index, we used different layers

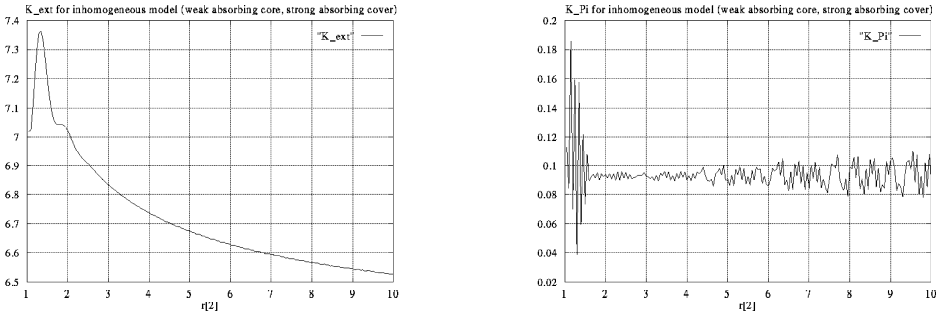

Fig. 6. Weak absorbing core and strong absorbing cover.

between core and cover, the so called interface, see figure 7 (left). This interface between core and cover, where the refractive indices decrease or increase in equidistant steps, approximates a linear gradient. We used three different interface regions with 2, 4 and 6 equidistant layers of variable width W where the refractive indices decrease or increase in 3, 5, or 7 equidistant steps. In

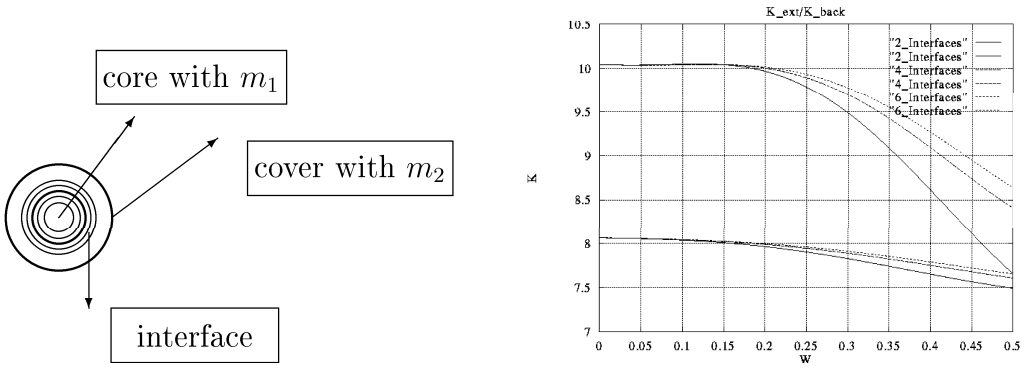

Fig. 7. Shell particle with 4 interface layers (left) and K_{ext} (lower three lines) and K_{π} (upper three lines) for different interfaces and variable width W of interfaces (right).

order to test the importance of the gradient shape, induced during the growth process of the particles, we considered an interface region of variable width W, where the refractive index decreases. Figure 7 shows the result for PSC II particle with a radius of $1.5\mu m$. The interface region between pure NAT and pure water is centered at 1 μm. The width of this interface is continuously varied from 0 μm to 0.5 μm. We examinate three different interface regions with different numbers of layers. We observe no significant differences for a width between 0 and 0.2 μm, which shows that the shape of the gradient and the number of layers are not critical. Differences become important above 0.3 μm. There is also an influence of the layer number. But it seems to be a quite good approximation with an interface of 6 layers.

5 Concluding remarks

Firstly, the scattering properties of natural inhomogeneous and only weak absorbing particles can be significantly different from those of homogeneous mixed or assumed non-absorbing equivalent spheres, thus suggesting that Mie theory may not be suitable for interpreting measurements particularly for anthropogenic tropospheric particles. Homogeneous-inhomogeneous, absorbing-nonabsorbing or both, respectively, differences in the extinction kernel and especially in the backscatter kernel of the first kind Fredholm integral equations of the lidar-operator (2) and (3) are very large and should be explicitly taken into account in inverting lidar measurements of tropospheric aerosols. Secondly, Mishchenko et al [12] observed the same effect when they examinated the shape of the particles. Dustlike tropospheric aerosol is not a spherical one. They determined the extinction and backscatter efficiency factors for a shape mixture of polydisperse, randomly oriented spheroids (prolates and oblates) using the so called T-matrix approach and compared the scattering and absorption properties of such non-spherical particles with projected-area-equivalent spheres. The computations clearly demonstrate that the extinction-to-backscatter ratio is highly sensitive not only to particle size and refractive index, but also to the particle shape. Rother [15] proposed a new numerically stable algorithm the so called discretized Mie-formalism for scattering on axisymmetric particles. The results fit very well with those obtained with the T-matrix approach.
The inevitable consequence of this high sensitivity is that Mie theory is inapplicable for inverting lidar measurements for non-spherical and inhomogeneous, absorbing particles. A modification and sensitivity study of the Mollifier inversion algorithm to solve the inverse ill-posed problem, see Böckmann et al [2], will be performed next using T-matrix approach, discrete Mie algorithm and Mie algorithm for projected-area-equivalent spheres.

References

[1] D. Baumgardner, J.E. Dye, B. Gandrud, K. Barr, K. Kelly, K.R. Chan, Refractive indices of aerosols in the upper troposphere and lower stratosphere, Geophysical Research Letters 23/7 (1996), 749-752.

[2] Ch. Böckmann, J. Biele, R. Neuber, Analysis of multi-wavelength lidar data by inversion with mollifier method, Pure Appl. Opt. 7 (1998) 827-836.

[3] Ch. Böckmann, Projection Method for Lidar Measurements, in: P. Ciarlini, M.G. Cox, F. Pavese, D. Richter (Eds.), Advanced Mathematical Tools in Metrology III, World Scientific, Singapore, 1997, pp. 239-240.

[4] Ch. Böckmann, J. Niebsch, Mollifier Methods for Aerosol Size Distribution, in: A. Ansmann, R. Neuber, P. Rairoux, U. Wandinger (Eds.), Advances in Atmospheric Remote Sensing with Lidar, Springer, New York, 1996, pp. 67-70.

[5] G.F. Bohren, D.R. Huffman, Absorption and Scattering of Light by Small Particles, John Wiley and Sons, New York, 1983.

[6] P. Chylek, G. Videen, D. Ngo, R.G. Pinnick, J.D. Klett, Effect of black carbon on the optical properties and climate forcing of sulfate aerosols, J. Geophys. Res. 100 (1995) 16325-16332.

[7] R. Courant, D. Hilbert, Methoden der mathematischen Physik, Springer, Berlin, Heidelberg, New York, 1993.

[8] G.H. Golub, C.F. van Loan, Matrix computations, John Hopkins University Press, Baltimore, London, 1989.

[9] B.R. Johnson, Light scattering by multilayer sphere, Applied Optics 35 (1996) 3286-3296.

[10] M. Kerker, The Scattering of Light and other electromagnetic radiation, Academic Press, New York, London, 1969.

[11] M.P. McCormick, L.W. Thomason, Atmospheric effects of the Mt. Pinatubo eruption, Nature 373 (1995) 399-404.

[12] M.I. Mishchenkow, L.D. Travis, R.A. Kahn, R.A. West, Modeling phase functions for dustlike tropospheric aerosols using a shape mixture of randomly oriented polydisperse spheroids, J. Geophys. Res. 102 (1997), 16831 - 16847.

[13] D. Müller, U. Wandinger, D. Althausen, I. Mattis, A. Ansmann, Retrieval of physical particle properties from lidar observations of extinction and backscatter at multiple wavelengths, Applied Optics 37 (1998) 2260-2263.

[14] J.M. Rosen, B.A. Bodhaine, J.F. Boatman, J.J. DeLuisi, M. J. Post, Y. Kim, R.C. Schnell, P.J. Sheridan, D.M. Garvey, Measured and calculated optical properties profiles in the mixed layer and free troposphere, J. Geophys. Res. 97 (1992), 12837 - 12850.

[15] T. Rother, Improvements of the discretized Mie-formalism for plane wave scattering on axisymmetric particles, J. Elec. Waves Appl. 11 (1997) 1033-1056.

[16] I. Schult, J. Feichter, W.F. Cooke,Effect of black carbon and sulfate aerosols on the global radiation budget, J. Geophys. Res. 102 (1997) 30107-30117.

[17] P. Stämpfli, P. Rairoux, B. Stein, J.P. Wolf, Scattering Properties of Inhomogeneous Polar Stratospheric Clouds, Preprint Freie Universität, 1995.

[18] Z.S. Wu, Y.P.Y. Wang, Electromagnetic scattering for multilayered sphere: recursive algoritms, Radio Sci. 26 (1991), 1393-1401.

[19] S.-C. Yoon, J.G. Won, Monitoring of atmospheric aerosols in Seoul using a micro pulse lidar, in: U.N. Singh, S. Ismail, G.K. Schwemmer (Eds.), Nineteenth International Laser Radar Conference, NASA/CP-1998-207671/PT1, Washington, 1998, pp. 83-85.